Catalytic mechanism of human glyoxalase i studied by quantum-mechanical cluster calculations

Jafari, Sonia; Ryde, Ulf; Irani, Mehdi

Published in:
Journal of Molecular Catalysis B: Enzymatic

DOI:
10.1016/j.molcatb.2016.05.010

2016

Document Version:
Peer reviewed version (aka post-print)

Catalytic mechanism of human glyoxalase I studied by quantum-mechanical cluster calculations

Sonia Jafari,[1] Ulf Ryde,[2] Mehdi Irani[1*]

[1] Department of Chemistry, University of Kurdistan, P.O. Box 66175-416, Sanandaj, Iran
[2] Department of Theoretical Chemistry, Lund University, P. O. Box 124, SE-221 00 Lund, Sweden

Abstract

Density functional theory has been used to study the mechanism and stereospecificity of the catalytic reaction of human glyoxalase I. We used the quantum mechanical cluster method to model the enzyme active site. Glyoxalase I accepts both enantiomers of the hemithioacetal between methylglyoxal and glutathione and converts them to the *S*-D enantiomer of lactoylglutathione. We have compared several previously suggested or alternative reaction mechanisms for both substrates on an equal footing. The results show that the coordination shell of the Zn ion in the optimized geometries is more symmetric than in some inhibitor crystal structures, which we assign to differences in the electronic structure and the protonation states. The symmetry of the active site model indicates that the enzyme can use the same reaction mechanism for the *S* and the *R* enantiomers of the substrate, but with exchanged roles of the two active-site glutamate residues. However, the calculations show some asymmetry (0–4 kcal mol^{-1} differences in reaction energies and activation barriers), caused by the different coordination states of the glutamate residues in the starting crystal structure. Our results indicate that the only possibility for the stereospecificity of GlxI is differences in the electrostatic surroundings and flexibility of the glutamate residues in the active site owing to their neighboring residues in the protein.

Keywords: Glyoxalase I, Mechanism, DFT, QM-cluster method, Stereospecificity

1. Introduction

Many enzyme substrates are chiral molecules and most enzymes catalyze reactions asymmetrically. In other words, most enzymes can only convert one enantiomer of a chiral substrate. For example, lipase B from *Candida antarctica* favors the *R* enantiomer of 1-phenylethanol.[1] However, there are enzymes with a different type of stereospecificity. Glyoxalase I (GlxI) is a paradigm of this behavior. GlxI takes both enantiomers of its chiral substrate, but converts them to a single enantiomer of the product. The enzyme is a part of glyoxalase system, which is composed of two enzymes (glyoxalase I and glyoxalase II) that catalyze the conversion of methylglyoxal (MG) to D-lactate. The system performs a critical two-step detoxification of cytotoxic MG. MG is produced naturally as a byproduct of normal biochemistry, but it is highly toxic due to its chemical reactions with proteins, nucleic acids, and other cellular components. GlxI, the subject of the present study, catalyzes the first step of the reaction, the conversion of the hemithioacetal of MG and glutathione (H-SG) to *S*-D-lactoylglutathione. The second detoxification step, in which the lactoylglutathione is split into glutathione and D-lactate, is carried out by glyoxalase II (Scheme 1).

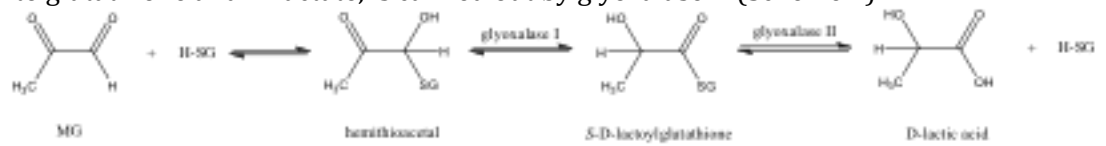

Scheme 1. The reaction catalyzed by the glyoxalase system. H-SG is glutathione.

It has been observed that GlxI is unusually active in various cancer cells and that MX is especially toxic to cancer cells [2]. Thus, the inhibition of GlxI could be a fruitful way to control tumors. An essential prerequisite to rational design of competitive inhibitors is detailed information about the active-site structure and reaction mechanism.

Human GlxI is a homodimer of 42 kDa, containing 183 amino acid residues per monomer

Scheme 1. The reaction catalyzed by the glyoxalase system. H-SG is glutathione.

It has been observed that GlxI is unusually active in various cancer cells and that MX is especially toxic to cancer cells [2]. Thus, the inhibition of GlxI could be a fruitful way to control tumors. An essential prerequisite to rational design of competitive inhibitors is detailed information about the active-site structure and reaction mechanism.

Human GlxI is a homodimer of 43 kDa, containing 183 amino acid residues per monomer. The enzyme has been crystallized with several inhibitors, like *S*-benzylglutathione (B-SG)[3] and *S*-[(*p*-nitrobenzyl)oxycarbonyl]glutathione (NBC-SG) [4]. However, the most interesting structure for the study of the catalytic mechanism is the complex with *S*-[*N*-hydroxy-*N*-(*p*-iodophenyl)carbamoyl] glutathione (HIC-SG) [4]. This inhibitor mimics the enediolate intermediate that has been suggested to be formed in the first step of the catalytic reaction [4-7]. According to the crystal structures, the active site of the enzyme consists of a shell of residues around a Zn^{2+} ion. In the resting human enzyme, His-126, Gln-33, Glu-99, Glu-172 and two water molecules are coordinated to the Zn^{2+} ion. When the inhibitor binds to the enzyme, it coordinates to the metal ion, displacing the two water molecules and Glu-172, giving a penta-coordinated site.

In 2001, three groups independently proposed two different mechanisms for the catalytic reaction of GlxI [5-7]. Richter and Krauss (RK) used HF/4-31G calculations of the active site, coupled with a frozen effective fragment potential description of eleven residues in the binding site [8,9] and proposed a three-step mechanism for the reaction of the *S* enantiomer of the substrate [5]. Himo and Siegbahn (HS) used density functional theory (DFT) and proposed a five-step mechanism for the *S* substrate [6] (the step counts exclude the binding of the substrate and the dissociation of the product). Creighton and Hamilton (CH) published a minireview, in which they discussed the catalytic reaction of GlxI as well as its stereospecificity [7]. They summarized experimental aspects of the catalytic mechanism of GlxI and suggested the same three-step mechanism as that proposed by RK. In addition, Åqvist and coworkers have also studied the first proton transfer with the empirical valence bond method [10].

Scheme 2 shows the mechanism for the *S* enantiomer of the substrate, proposed by RK and CH. The reaction starts with abstraction of H1 by Glu-172 (see Scheme 2 for the numbering of the atoms). Then, H1 is transferred from Glu-172 to C2 and concurrently H2 is transferred from O1 to Glu-99. Finally, H2 is transferred from Glu-99 to O2 and the product is formed.

The first step of this mechanism is also the first step of the mechanism proposed by HS. However, in the second step of the latter mechanism, H1 moves from Glu-172 to O2 (*Scheme 3*). Next, the resulting intermediate is transformed to an isoenergic structure, in which H1 binds to O1 and H2 binds to O2, but the hydrogen bonds with Glu-99 and Glu-172 are kept (these hydrogen bonds are indicated by dotted lines in Scheme 3). After that, Glu-172 abstracts H1 from O1 and finally transfers it to C2.

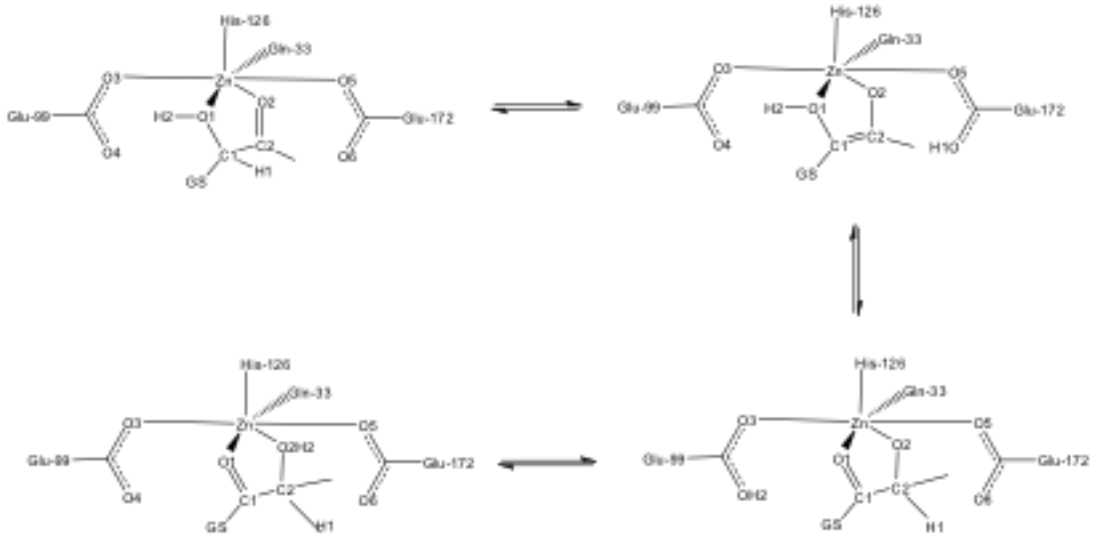

Scheme 2. Schematic view of the RKCH mechanism reaction of GlxI for the *S* substrate (excluding the binding of the substrate to and the dissociation of the product from the active site).

Scheme 2. Schematic view of the RKCH mechanism reaction of GlxI for the *S* substrate (excluding the binding of the substrate to and the dissociation of the product from the active site).

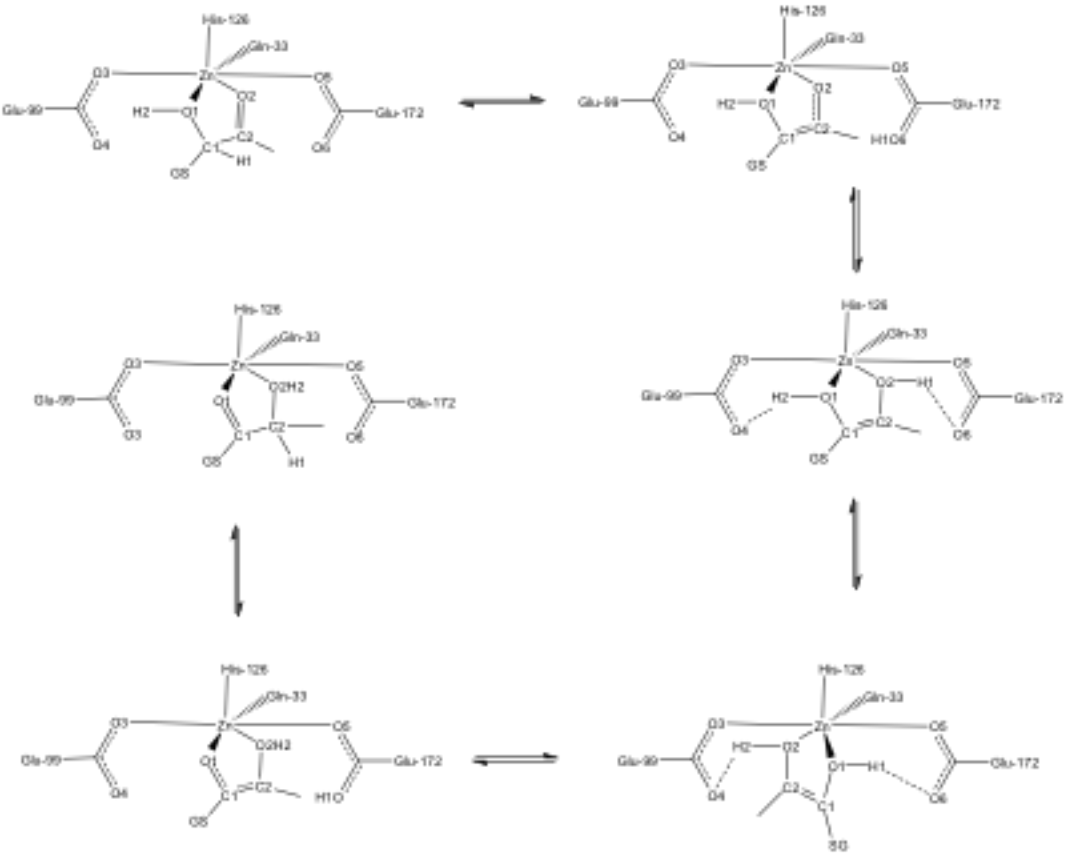

Scheme 3. Schematic view of the HS mechanism of GlxI for the *S* substrate. The hydrogen-bond patterns of H1 and H2 with Glu-99 and Glu-172 in the isoenergic structures are indicated by dotted lines.

The most challenging part in the catalytic mechanism of GlxI is its stereospecificity and the reaction of the *R* substrate. The first step of the proposed mechanisms for the *R* substrate in the various works is same, viz. the abstraction of H1 by Glu-99 [4-7]. However, the three groups proposed different steps for the subsequent reaction. RK suggested that in the second step, Glu-172 receives H2 and transfers it to C2, whereas H1 goes to O2 (Scheme 4). HS proposed that after the first step, H1 moves to O2. Then, Glu-172 abstracts H2 from O1 and transfers it to the *si* face of C2 to produce the product (Scheme 5). CH proposed a dissociative mechanism for the *R* substrate, i.e. that the enzyme first converts the *R* substrate to the *S* substrate (via a dissociation of a glutathionyl mercaptide ion) and then processes the *S* substrate (Scheme 6).

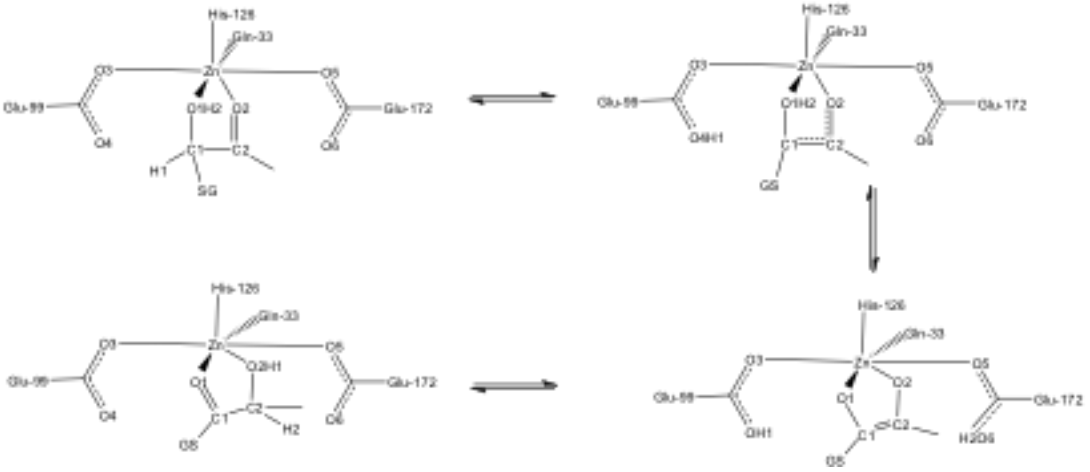

Scheme 4. Schematic view of the RK mechanism for the *R* substrate of GlxI.

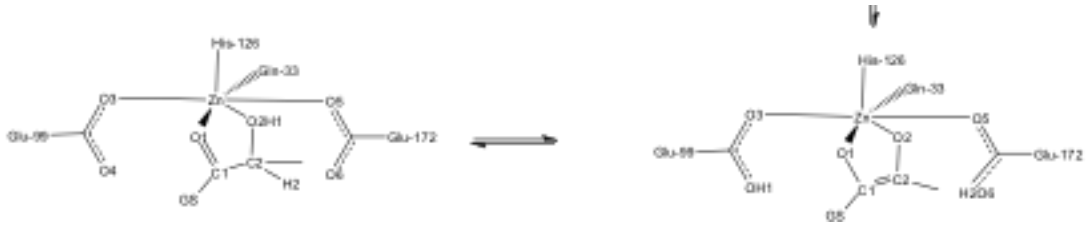

Scheme 4. Schematic view of the RK mechanism for the *R* substrate of GlxI.

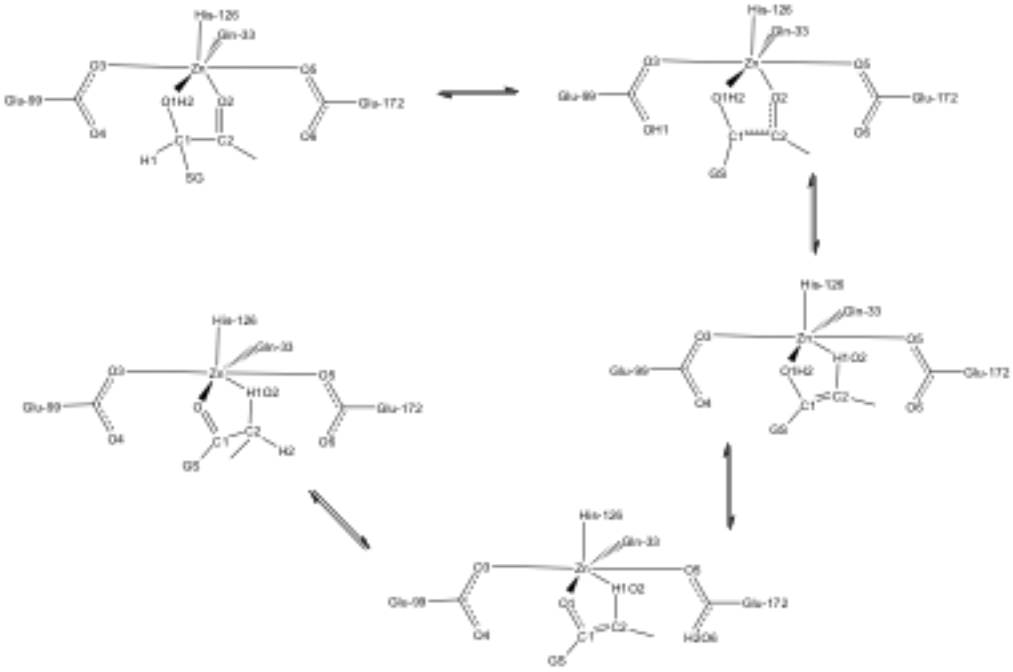

Scheme 5. Schematic view of the HS mechanism for the *R* substrate of GlxI.

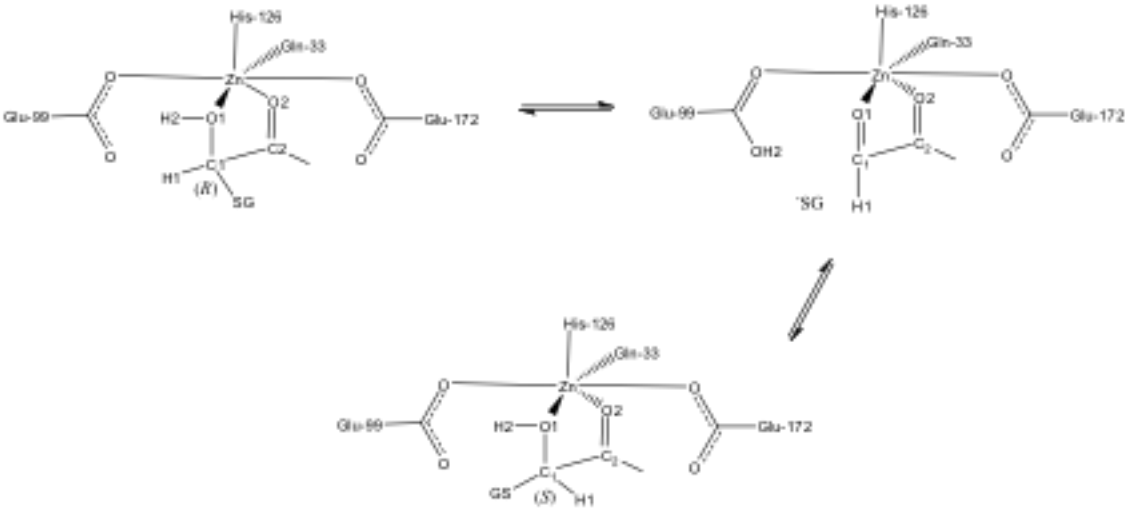

Scheme 6. The dissociative CH mechanism for the *R* substrate of GlxI.

Thus, despite all the previous studies, details of the reaction mechanism and the stereospecificity of GlxI are still unknown. In this paper, we investigate all proposed mechanisms for both the *S* and *R* substrates on an equal footing. We have used the quantum mechanical (QM) cluster approach, which has extensively been used to study catalytic mechanisms and structures of enzymes [11-26]. In this approach, the most important residues are cut out from the active site of the enzyme. It reduces the number of considered atoms to 50–200, which makes it possible to study the reaction by DFT methods. In order to avoid that the model may change significantly from the crystal structure during the geometry optimization, some atoms are kept fixed at their crystal-structure positions. In addition, to account for the protein surrounding, continuum-solvation techniques are used, which

stereospecificity of GlxI are still unknown. In this paper, we investigate all proposed mechanisms for both the *S* and *R* substrates on an equal footing. We have used the quantum mechanical (QM) cluster approach, which has extensively been used to study catalytic mechanisms and structures of enzymes [11-26]. In this approach, the most important residues are cut out from the active site of the enzyme. It reduces the number of considered atoms to 50–200, which makes it possible to study the reaction by DFT methods. In order to avoid that the model may change significantly from the crystal structure during the geometry optimization, some atoms are kept fixed at their crystal-structure positions. In addition, to account for the protein surrounding, continuum-solvation techniques are used, which model the surrounding as a homogenous polarizable medium, characterized by a dielectric constant. The choice of this constant is somewhat arbitrary, but $\varepsilon = 4$ is usually considered to be a good representation of protein surrounding [27-33].

2. **Computational Details and modeling**

All calculations were performed using the density functional B3LYP [34] method, implemented in Gaussian03 [35] program. The structures of reactants, transition states, intermediates, and products were optimized using the 6-31+G(d) basis set for the H, C, N, O and S atoms and the LANL2DZ basis set [36] for the Zn ion. Accurate energies were calculated with single-point calculations on the optimized structures using the larger 6-311++G(2d,2p) basis set for all atoms. This is the same DFT method as used by HS,[6] but the basis sets are slightly larger, both those used for geometries and for energies. It is much more accurate than the HF/4-31G calculations performed by RK.[5] To consider the surroundings, solvation effects were evaluated at the B3LYP/6-31+G(d)/LANL2DZ level of theory by performing single-point calculations using the CPCM solvation model [37]. The CPCM calculations used UFF atomic radii and default water solvent parameters, but the dielectric constant was set to 4. Natural orbital bond (NBO) analysis [38,39] was used to calculate atomic charges on the optimized structures. The NBO calculations were performed at the same level of theory as the single-point energy calculations. Frequencies of the stationary states on the potential energy surfaces were calculated to obtain zero-point energies. The frequency calculations were performed at the same level of theory as the geometry optimizations. All energies discussed in this article include zero-point energies and the electrostatic part of the solvation energy.

A model of the active site of human GlxI was constructed based on the HIC-SG crystal structure of the native enzyme (Protein Data Bank entry 1QIN) [4]) . The model consists of the zinc atom, and its first coordination shell amino acids (Gln-33, Glu-99, Glu-172 and His-126), as well as the inhibitor. The amino acid residues were truncated so that only the side chains were kept in the model. Thus, the glutamates were represented by propionate, glutamine by propanamide and histidine by methyl-imidazole. The inhibitor was modified to a model of the substrate: The para-iodophenyl group was replaced by a methyl group, the N atom next to the iodophenyl group by a carbon atom and the -SG group by a -SH group. Hydrogen atoms were added manually. To maintain the overall structure of the active site, the carbon atoms bound to the H atoms that truncated the active site amino acids were fixed at their corresponding positions from the crystal structure during the geometry optimizations. The model and the fixed atoms are shown in Figure 1.

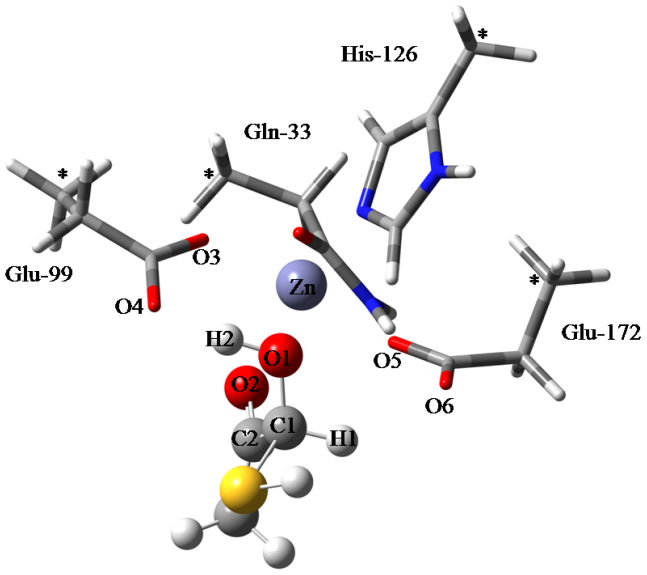

Figure 1. Optimized model of the active site with the *S* substrate (***S*-R**). The fixed atoms are marked with asterisks.

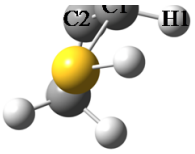

Figure 1. Optimized model of the active site with the *S* substrate (***S*-R**). The fixed atoms are .marked with asterisks

3. Results and Discussion

To gain some understanding of the catalytic mechanism and stereospecificity of GlxI, we have performed DFT calculations on both the *S* and *R* enantiomers of the substrate in the active-site model. We discuss the results for each of these enantiomers in separate subsections.

3.1. Reaction mechanism of the *S* substrate

Figure 1 shows the optimized structure of the reactant state of the *S* substrate (***S*-R**) and selected geometrical parameters are listed in Table 1. The results show that the coordination shell of the Zn ion in the optimized geometry is different from the starting crystal structure (HIC-SG structure): In the optimized structure, the Zn ion is coordinated to six atoms, two from the substrate and one each from the models of Gln-33, His-126, Glu-99, and Glu-172. However, in the HIC-SG crystal structure, Glu-172 does not bind to the Zn ion (the Zn–O5 and Zn–O6 distances are 3.27 and 4.27 Å, compared to 2.12 and 3.50 Å in the optimized structure; atom names are shown in Figure 1; C1, C2, H1, H2, O1 and O2 are the atoms of the substrate that directly participate in the reaction; O3 and O4 are the oxygen atoms of the carboxyl group of Glu-99; O5 and O6 are the oxygen atoms of the carboxyl group of Glu-172; the O3 and O5 atoms coordinate to the Zn ion). On the other hand, the optimized structure of ***S*-R** is similar to B-SG and NBC-SG crystal structures, in which one and two water molecules coordinate to the Zn ion, respectively (but not the inhibitor), and the glutamates symmetrically coordinate to the zinc atom (the Zn–O3 and Zn–O5 distances are 1.98 & 2.02 Å and 2.04 & 1.97 Å in B-SG and NBC-SG crystal structures, respectively, compared to 2.04 and 2.12 Å in the optimized structure). In HIC-SG crystal structure, the inhibitor is directly coordinated to the Zn atom with two oxygen atoms. The difference between the optimized structure and HIC-SG structure could be related to different electronic effects and the protonation states of the substrate and the inhibitor. RK [5] used the B-SG crystal structure for their calculations. They showed that if the two glutamate ligands are free to move during the optimization, the protonated Glu-172 will dissociate from the zinc ion (in the first intermediate of the reaction), and the resulting structure will be similar to the HIC-SG crystal structure. They suggested that Glu-172 is protonated also in the HIC-SG/GlxI complex and that the inhibitor must be negatively charged, because otherwise the enediolate intermediate analogue would not bind as strongly to the metal center as it is seen in the HIC-SG crystal structure [4]. In fact, the C2 atom of the substrate is in the HIC-SG/GlxI complex replaced by a more electronegative nitrogen atom that is connected to an iodophenyl group. This makes H1 a better leaving group. Thus, Glu-172 may abstract H1 from the inhibitor in HIC-SG crystal structure and dissociate from the Zn ion (the inhibitor has an *S* stereochemistry in C1 position, so that H1 is directed towards Glu-172 and not to Glu-99). Our results show that in the first intermediate of the *S* substrate reaction (***S*-IM1**), in which Glu-172 is protonated, the Zn–O5 distance is longer than in the other stationary states (i.e., 2.23 Å compared to 2.12 Å in ***S*-R**; see Table 1 for distances in the other stationary points). In conclusion, the available data suggest that Glu-172 is protonated in the HIC-SG complex. HS obtained a similar six-coordinated ***S*-R** structure in their calculations [6].

Table 1. Structural parameters for the optimized first-order stationary points and the crystal structures (distances in Å).

	***S*-R**	***S*-IM1**	***S*-IM2**	***D*-P**	***R*-R**	***R*-IM1**	X-ray		
							HIC-SG[4a]	B-SG[3]	NBC-SG[4]
C1-C2	1.54	1.38	1.54	1.54	1.53	1.38	...	...	...
C1-O1	1.40	1.41	1.22	1.21	1.40	1.41	...	...	...
C2-O2	1.22	1.31	1.38	1.41	1.24	1.31	...	...	...
C1-H1	1.10	2.05	...	...	1.09	2.09	....	....	....
O4-H1	...	...	...	...	2.47	1.00	...	...	...
O6-H1	2.20	1.00	3.62	2.42	...	...	...	...	...
C2-H1	...	2.20	1.10	1.10					

							HIC-SG[4a]	B-SG[3]	NBC-SG[4]
C1-C2	1.54	1.38	1.54	1.54	1.53	1.38	…	…	…
C1-O1	1.40	1.41	1.22	1.21	1.40	1.41	…	…	…
C2-O2	1.22	1.31	1.38	1.41	1.24	1.31	…	…	…
C1-H1	1.10	2.05	…	…	1.09	2.09	….	….	….
O4-H1	…	…	…	…	2.47	1.00	…	…	…
O6-H1	2.20	1.00	3.62	2.42	…	…	…	…	…
C2-H1	…	2.29	1.10	1.10	…	…	…	…	…
O1-H2	1.05	1.01	1.79	…	1.02	1.03	…	…	…
O4-H2	1.50	1.67	0.99	1.55	…	…	…	…	…
O6-H2	…	…	…	…	1.57	1.58	…	…	…
O2-H2	…	…	2.61	1.03	…	1.02	…	…	…
Zn-O1	2.20	2.23	3.83	2.42	2.26	2.22	2.04/2.09	…	…
Zn-O2	2.30	2.06	1.94	2.17	2.26	2.04	2.13/2.14	…	…
Zn-O3	2.04	2.02	2.80	2.08	2.02	2.28	1.91/1.89	1.98	2.04
Zn-O4	3.36	3.28	4.08	3.39	3.49	3.80	3.00/2.97	3.04	3.28
Zn-O5	2.12	2.23	1.99	2.04	2.06	2.05	3.25/3.27	2.02	1.97
Zn-O6	3.50	3.80	3.23	3.50	3.39	3.30	4.18/4.27	3.48	3.56
Zn-His[b]	2.10	2.13	2.05	2.10	2.11	2.11	2.05/2.10	2.02	2.13
Zn-Gln[c]	2.12	2.11	2.03	2.09	2.14	2.12	2.05/1.99	2.00	1.93

.[a] Two distances are given because there are two subunits in the crystal structure
[b] The distances between the Zn ion and the NE2 atom of His-126.
.[c] The distances between the Zn ion and the OE1 atom of Gln-33

As discussed above, the first step in all proposed catalytic mechanisms of GlxI is a proton transfer from C1 to Glu-172 [4-6,40], giving rise to an enediolate intermediate (***S*-IM1**). In the optimized ***S*-R** structure, Glu-172 is located at a proper position to abstract H1 (H1 is directed towards O6; cf. Figure 1). The long Zn–O6 distance (3.50 Å) makes O6 a stronger nucleophile than the coordinated O5 in ***S*-R**. In the optimized structure of the transition state for this step (***S*-TS1**), the C1–H1 and H1–O6 distances are 1.52 and 1.14 Å, respectively. The energy barrier for this step is 11.4 kcal mol^{-1} and the ***S*-IM1** intermediate is 9.1 kcal mol^{-1} higher than ***S*-R**. These energies are somewhat different from what was obtained in the other computational works. The RK results indicated that the intermediate was 4.8 and 13.3 kcal mol^{-1} higher than the reactant when the CA atoms of the glutamate residues were unfrozen and frozen, respectively [5]. According to HS, the transition state and the intermediate are 14.4 and 12.6 kcal mol^{-1} higher than the reactant, respectively [6]. On the other hand, Åqvist et al. [10] found that the reaction is nearly thermoneutral and the barrier is ~13 kcal mol^{-1}. HS proposed that the discrepancy in the energies between the latter two investigations could originate from problems in Åqvist's molecular-mechanics parameterization of the metal site. The discrepancy between our results and those of HS could originate from the different model size and the fixing pattern of atoms (each amino acid in the HS model had one methylene group less and they did not fix any atom during the optimizations).

A number of geometrical and electronic changes takes place when going from ***S*-R** to ***S*-IM1** via ***S*-TS1** and provides important chemical information about the reaction. The single C1–C2 bond is shortened from 1.54 to 1.38 Å and the double C2=O2 bond is elongated from 1.22 to 1.31 Å (cf. Table 1). In addition, the increased negative charge on O2 (from –0.58 in ***S*-R** to –0.86 in ***S*-IM1**) leads to a stronger coordination of O2 to the Zn atom (the Zn–O2 distances are 2.30 and 2.06 Å for ***S*-R** and ***S*-IM1**, respectively). These results demonstrate that the active-site Zn ion provides catalytic power by stabilizing the developing negative charge on O2 of the enediolate intermediate. This is in line with the results of Åqvist et al. [10], who concluded that the main catalytic role of the Zn ion is to electrostatically stabilize the endiolate intermediate, thereby lowering the activation free energy of proton transfer. The .optimized structures of the stationary points are shown in Figure 2

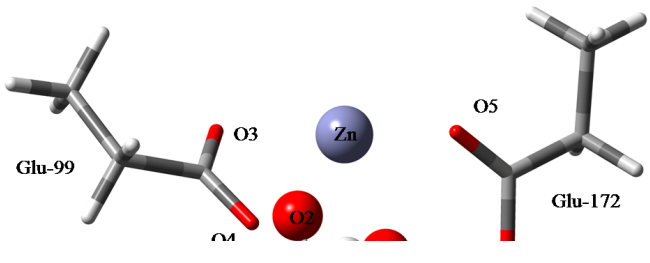

.optimized structures of the stationary points are shown in Figure 2

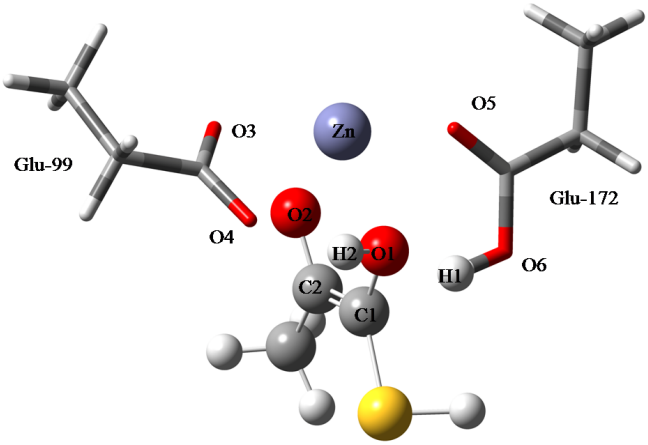

***S*-IM1**

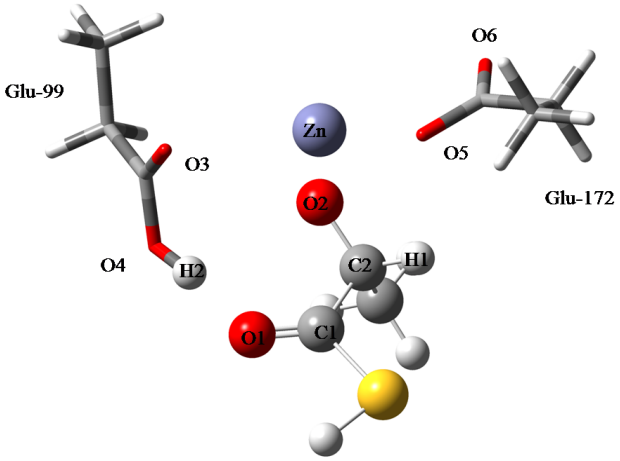

***S*-IM2**

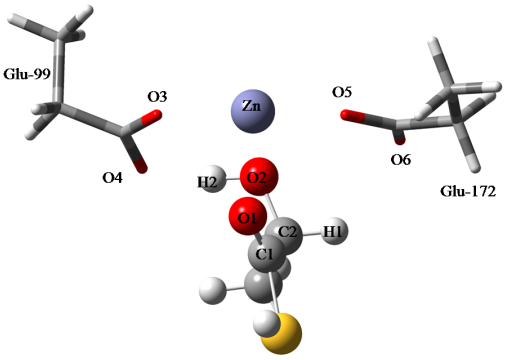

D-**P**

Figure 2. Optimized structures of the stationary points along the reaction pathway for the *S* substrate. For clarity, only the Zn atom, the substrate and the glutamate residues are shown.

After the first step, there are three possibilities how the reaction may proceed: transfer of H2 to Glu-99, immediate transfer of H1 from Glu-172 to C2 (second step of the RKCH mechanism) or transfer of H1 to O2 (second step of the HS mechanism). We have tested all three possibilities. However, the transfer of H2 to Glu-99 did not lead to any stable intermediate (all optimized structures return to ***S*-IM1**). This is quite natural, because it would give rise to a double negative charge on the substrate.

On the other hand, ***S*-IM1** has appropriate properties for the transfer of H1 to C2: The H1–C2 distance is 2.29 Å and the charge on C2 is less positive than that in ***S*-R** (0.34 vs. 0.59). Therefore, we scanned the C2–H1 distance in steps of 0.2 Å, optimizing the structures along the reaction path. The results showed that while H1 moves to C2, H2 concertedly moves from O1 to O4, leading to a double bond between C1 and O1 in the corresponding intermediate, ***S*-IM2**. The energy barrier for this step is quite high, 12.4 kcal mol^{-1}, and the transition state (***S*-TS2**) is 21.5 kcal mol^{-1} higher than ***S*-R** (the optimized structures of the stationary points and the energy profile are shown in Figure 2 and Figure 3, respectivly). The reaction is exothermic by –5.9 kcal mol^{-1} and ***S*-IM2** is 3.2 kcal mol^{-1} above ***S*-R**. As the C1–O1 double bond is formed, the O1–Zn bond is cleaved (the Zn–O1 distance goes from

C2 distance is 2.29 Å and the charge on C2 is less positive than that in ***S*-R** (0.34 vs. 0.59). Therefore, we scanned the C2–H1 distance in steps of 0.2 Å, optimizing the structures along the reaction path. The results showed that while H1 moves to C2, H2 concertedly moves from O1 to O4, leading to a double bond between C1 and O1 in the corresponding intermediate, ***S*-IM2**. The energy barrier for this step is quite high, 12.4 kcal mol^{-1}, and the transition state (***S*-TS2**) is 21.5 kcal mol^{-1} higher than ***S*-R** (the optimized structures of the stationary points and the energy profile are shown in Figure 2 and Figure 3, respectivly). The reaction is exothermic by –5.9 kcal mol^{-1} and ***S*-IM2** is 3.2 kcal mol^{-1} above ***S*-R**. As the C1–O1 double bond is formed, the O1–Zn bond is cleaved (the Zn–O1 distance goes from 2.23 Å in ***S*-IM1** to 3.83 Å in ***S*-IM2**).

To produce the D-product (**D-P**), O2 has to accept a proton to complete its valance. The hydrogen atom H2, which is on O4 in ***S*-IM2**, is in an appropriate position to move to O2. The negative charge on O2 in ***S*-IM2** (–0.98) shows its affinity to abstract a proton. Our calculations show that such a proton transfer is quite facile: The reaction is exothermic by –9.2 kcal mol^{-1} and it leads to formation of **D-P**. We have optimized the TS (***S*-TS3**) for this step, but when all corrections were taken into account (large basis set, ZPE, solvation and dispersion), the energy of the TS was found to be 0.1 kcal mol^{-1} lower than the energy of ***S*-IM2**. This is of course an artifact of the adopted methodology (i.e., optimizing in the gas phase with a medium-sized basis set and adding all corrections based on that geometry), as has previously been observed in several cases [11-13], but it shows that the reaction is facile. During the reaction, the Zn–O1 bond is reformed, although it is quite weak (2.42 Å).

The two later steps illustrate the role of Glu-99 in the catalytic reaction. Glu-99 abstracts H2 from O1 and then delivers it to O2, in line with a mutation study, showing that the E99Q mutant of human GlxI had a 10^4-fold decreased enzyme activity [40]. In fact, Glu-99 acts as a ping-pong table in the catalytic mechanism, with H2 as the ball and O1 and O2 as the players. These results show that the RKCH mechanism is possible, but with a quite high total activation barrier of 21.5 kcal mol^{-1} and a reaction energy of –6.0 kcal mol^{-1}, see Figure 3. The calculations also give a detailed description of the geometries of the involved intermediates and transition states.

Figure 3. The calculated potential energy profile for the *S* substrate of the different studied mechanisms.

9

Finally, we tested also the HS mechanism, involving a transfer of H1 to O2 in ***S*-IM1**. The results show that this step can take place with a small barrier (1.0 kcal mol^{-1}) and the resulting intermediate (***S*-IM2H**) is 4.4 kcal mol^{-1} higher than ***S*-R**. In ***S*-IM2H**, Glu-99 forms a short hydrogen bond to H2, suggesting that this residue may abstract the second proton. However, this would result in the wrong enantiomer of the product when the proton is delivered to C2. Still, we tested this path (it is important to test all possible mechanisms and show that alternative paths are less favorable) and the energy profile is shown in green in Figure 3. This path first crosses a shallow well (***S*-IM3H-L**, the TS is ***S*-TS3H-L**), in which the H2 proton is transferred to Glu-99 (structures are shown in Figure 4). Then, H2 moves to C2, giving the L enantiomer of the product (**L-P**). This second step involves a higher energy barrier (7.9 and 12.7 kcal mol^{-1} above ***S*-IM3H-L** and ***S*-R**, respectively), because the proton is sandwiched between O1 and O6 in ***S*-IM3H-L**. The product (**L-P**) is –5.2 kcal mol^{-1} below ***S*-R** and therefore is close in energy to the **D-P** product (cf. Figure 3).

To instead obtain **D-P**, HS used an isoenergic structure of ***S*-IM2H** (here called ***S*-IM2H-ISO**) in which H1 has moved from O2 to O1 and H2 has moved from O1 to O2, but both protons keep their hydrogen bonds to the glutamate residues (H1 forms a hydrogen bond to Glu-172 and H2 forms a hydrogen bond to Glu-99; cf. Figure 4; alternatively, it can be seen as a rotation of both protons on the substrate O atoms ~180° around the C–O axis). Our calculations confirm that this structure (***S*-IM2H-ISO**) has the same energy as ***S*-IM2H** (owing to the symmetry of the QM-cluster models). In the third step of their proposed mechanism, Glu-172 abstracts H1 from O1 in ***S*-IM2H-ISO**, giving the intermediate, ***S*-IM3H** via ***S*-TS3H**. The energy barrier for this step is only 0.3 kcal mol^{-1} and ***S*-IM3H** is 0.5 kcal mol^{-1} higher than ***S*-IM2H** and ***S*-IM2H-ISO**. The energies seem reasonable because it is a simple hydrogen-bond exchange between two oxygen atoms, which apparently have a similar basicity. Finally, H1 is transferred to C2 to produce **D-P**. The TS of the last step (**S-**

172 and H2 forms a hydrogen bond to Glu-99; cf. Figure 4; alternatively, it can be seen as a rotation of both protons on the substrate O atoms ~180° around the C–O axis). Our calculations confirm that this structure (***S*-IM2H-ISO**) has the same energy as ***S*-IM2H** (owing to the symmetry of the QM-cluster models). In the third step of their proposed mechanism, Glu-172 abstracts H1 from O1 in ***S*-IM2H-ISO**, giving the intermediate, ***S*-IM3H** via ***S*-TS3H**. The energy barrier for this step is only 0.3 kcal mol^{-1} and ***S*-IM3H** is 0.5 kcal mol^{-1} higher than ***S*-IM2H** and ***S*-IM2H-ISO**. The energies seem reasonable because it is a simple hydrogen-bond exchange between two oxygen atoms, which apparently have a similar basicity. Finally, H1 is transferred to C2 to produce **D-P**. The TS of the last step (***S*-TS4H**) is 5.7 and 10.6 kcal mol^{-1} above ***S*-IM3H** and ***S*-R**, respectively.

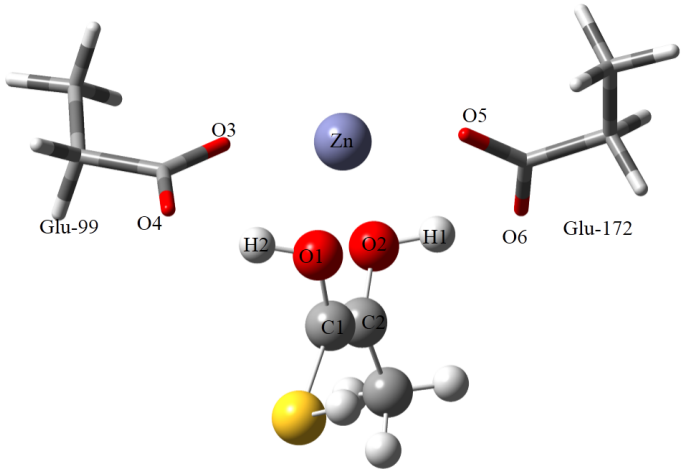

***S*-IM2H**

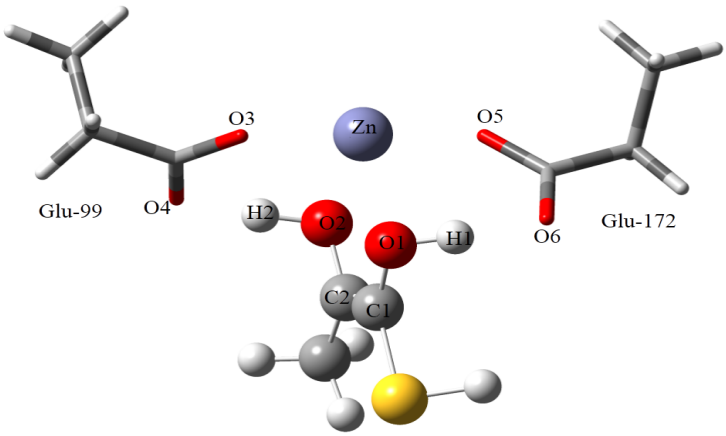

***S*-IM2H-ISO**

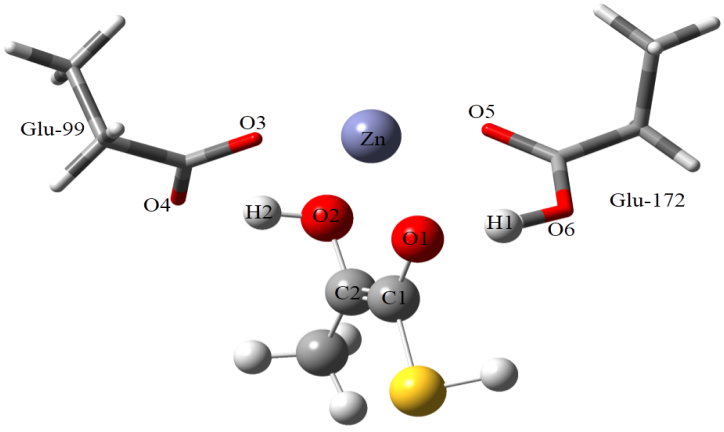

***S*-IM3H**

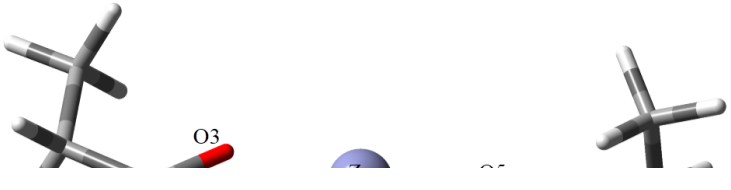

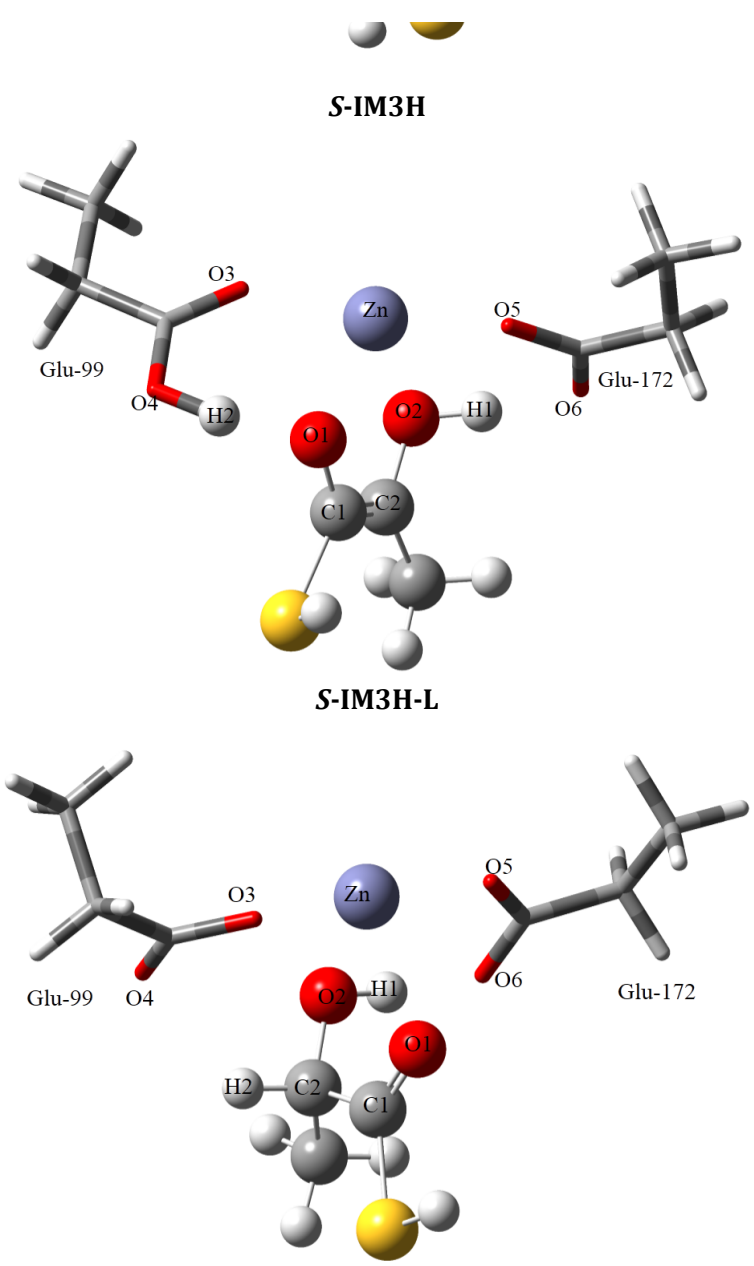

Figure 4. Optimized structures of the stationary points along the reaction pathway for the *S* substrate in the HS mechanism and the alternative path leading to the other **L-P** product. For clarity, only the Zn atom, the substrate and the glutamate residues are shown.

A problem with the HS mechanism is that only one of the active-site glutamates (Glu-172) performs all catalytic steps, whereas the other glutamate (Glu-99) has no direct role in the catalytic mechanism. This is not in line with the mutation studies, showing that the E99Q mutant of human GlxI had a 10^4-fold decrease in enzyme activity [40]. In addition, it is not clear how the isoenergic structures (***S*-IM2H** and ***S*-IM2H-ISO**) can be transformed to each other. In this transformation, two hydrogen bonds must be exchanged and two dihedrals in the glutamates (O4-CD-CG-CB in Glu-99 and O6-CD-CG-CB in Glu-172) must be rotated about 180°. This transformation is thermoneutral but it may pass through high barriers. In other words, the isoenergic structures are not necessarily connected in any easy way – both H atoms need to be abstracted by the two glutamate residues (which we have already shown is unfavorable) and then added back on the other O atom.

We have tried to model this transformation in five separated steps (with five TSs and four additional intermediates). We first moved H2 to O4 (resulting in ***S*-IM2H-im1** via ***S*-IM2H-ts1**) and then rotated Glu-99 so that H2 interacts with O2 (giving ***S*-IM2H-im2** via ***S*-IM2H-ts2**). Next, we moved H2 to O2 (H1 moves at the same time to O6; resulting in ***S*-IM2H-im3** via ***S*-IM2H-ts3**). After that, we rotated H1 so that it interacts with O1 (giving ***S*-IM2H-im4** via ***S*-IM2H-ts4**). Finally we moved H1 to O1 (resulting in ***S*-IM2H-ISO** via ***S*-IM2H-ts5**). The first-order stationary structures are shown in Figure 5 and the energy profile of these steps is shown in Figure 3.

The results show that the second and fourth steps of this transformation (rotation of Glu-99 so that H2 interacts with O2 and rotation of Glu-172 so that H1 interacts with O1) have quite high barriers (9.2 and 6.2 kcal mol^{-1}, respectively). In fact, the TS of the fourth step has the highest energy among the stationary points connecting **S-P** and **D-P** (14.3 kcal mol^{-1}).

ts2). Next, we moved H2 to O2 (H1 moves at the same time to O6; resulting in ***S*-IM2H-im3** via ***S*-IM2H-ts3**). After that, we rotated H1 so that it interacts with O1 (giving ***S*-IM2H-im4** via ***S*-IM2H-ts4**). Finally we moved H1 to O1 (resulting in ***S*-IM2H-ISO** via ***S*-IM2H-ts5**). The first-order stationary structures are shown in Figure 5 and the energy profile of these steps is shown in Figure 3.

The results show that the second and fourth steps of this transformation (rotation of Glu-99 so that H2 interacts with O2 and rotation of Glu-172 so that H1 interacts with O1) have quite high barriers (9.2 and 6.2 kcal mol^{-1}, respectively). In fact, the TS of the fourth step has the highest energy among the stationary prints connecting ***S*-R** and **D-P** (14.3 kcal mol^{-1}). Thus, the overall barrier of production of **D-P** from ***S*-R** is slightly higher than the overall barrier of production of **L-P** from ***S*-R**, owing to the barrier connecting the isoenergic structures (14.3 vs. 12.7 kcal mol^{-1}). This shows that the production of the wrong enantiomer of the product is more favorable than production of the right enantiomer of the product for the considered nearly symmetric QM-cluster model. On the other hand, both reactions have appreciably lower barriers than the RKCH mechanism (21.5 kcal mol^{-1}), showing that the latter is an unlikely mechanism for the *S* substrate. Finally, we note that the isomerization of ***S*-IM2H** to ***S*-IM2H-ISO** involves Glu-99, showing that that residue is actually also needed for the HS mechanism, in agreement with the mutation studies [41].

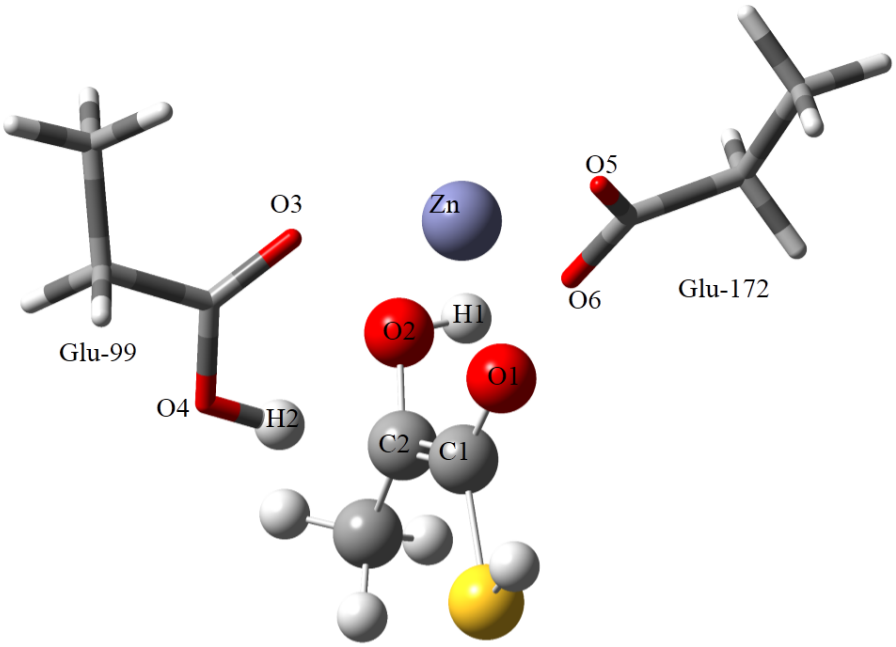

***S*-IM2H-im1**

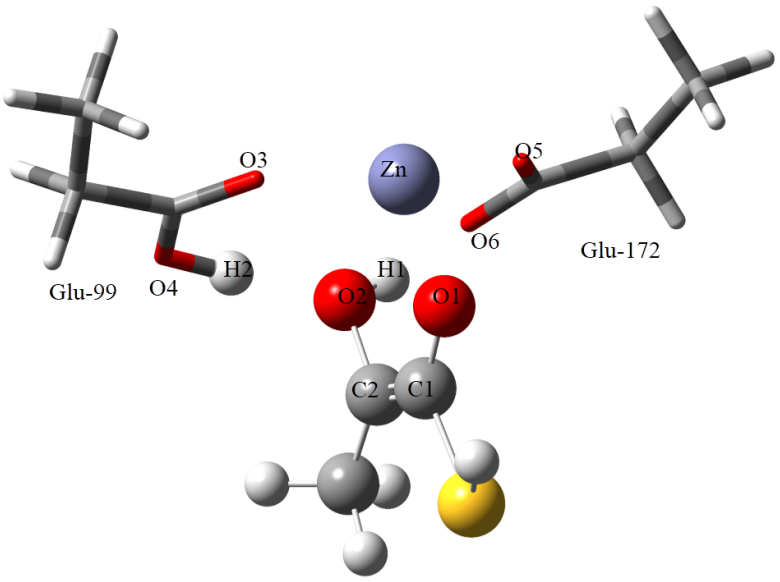

***S*-IM2H-im2**

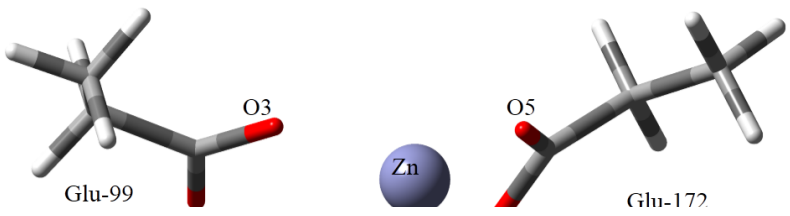

***S*-IM2H-im2**

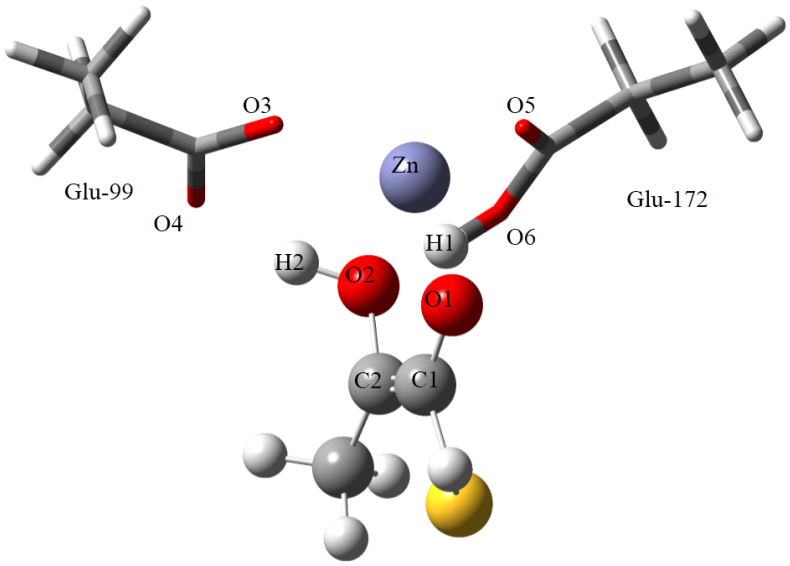

***S*-IM2H-im3**

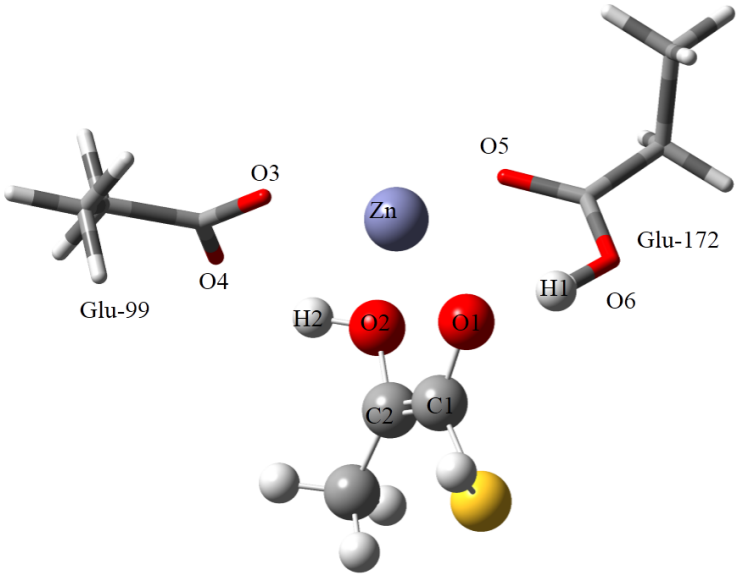

***S*-IM2H-im4**

Figure 5. Optimized structures of the stationary points along the reaction pathway connecting ***S*-IM2H** to ***S*-IM2H-ISO**. For clarity, only the Zn atom, the substrate and the glutamate residues are shown.

3.2. Reaction steps for the *R* substrate

To study the *R* substrate reaction, the stereochemistry of the substrate model was changed in the C1 position (H1 was transferred from the *si* face to the *re* face of C1). The optimized structure of the reactant for the *R* substrate (***R*-R**) is shown in Figure 6. Like the *S* substrate, the Zn ion is six-coordinate with both Glu-99 and Glu-172 coordinating (the calculated Zn–O3 and Zn–O5 distances are 2.02 and 2.06 Å, respectively). The proposed first step in the reaction of the *R* substrate is abstraction of H1 from C1 by Glu-99 [3-7], leading to the enediolate intermediate ***R*-IM1**, via the transition state ***R*-TS1**. The structure of the transition state and its energy are only slightly different to those of the *S* enantiomer. The energy barrier is 10.5 kcal mol^{-1} (11.4 kcal mol^{-1} for the *S* substrate) and ***R*-IM1** is 7.1 kcal mol^{-1} higher than the reactant (9.1 kcal mol^{-1} for the *S* substrate, see Figure 8 for the energy profile). In ***R*-IM1**, the Zn–O3 distance (to Glu-99) is longer than the Zn–O5 distance (to Glu-172), whereas the opposite was true in ***S*-IM1** (see Table 1). This illustrates the exchanged roles of Glu-172 and Glu-99 in the catalytic mechanism of *S* and *R* substrates. However, most of the corresponding distances in ***S*-R** & ***R*-R** and in ***S*-IM1** & ***R*-IM1** are very close, although the energy profile for the first step of the *S* and *R* enantiomers differs slightly. The latter difference is related to some geometrical parameters involving the glutamate groups (e.g. O6–H1 is 2.20 Å in ***S*-R** whereas O4–H1 is 2.47 Å in ***R*-R**, and O4–H2 is 1.67 Å in ***S*-IM1** and O6–H2 is 1.58 Å in ***R*-IM1**), which in turn is caused by the different positions of the

profile). In ***R*-IM1**, the Zn–O3 distance (to Glu-99) is longer than the Zn–O5 distance (to Glu-172), whereas the opposite was true in ***S*-IM1** (see Table 1). This illustrates the exchanged roles of Glu-172 and Glu-99 in the catalytic mechanism of *S* and *R* substrates. However, most of the corresponding distances in ***S*-R** & ***R*-R** and in ***S*-IM1** & ***R*-IM1** are very close, although the energy profile for the first step of the *S* and *R* enantiomers differs slightly. The latter difference is related to some geometrical parameters involving the glutamate groups (e.g. O6–H1 is 2.20 Å in ***S*-R** whereas O4–H1 is 2.47 Å in ***R*-R**, and O4–H2 is 1.67 Å in ***S*-IM1** and O6–H2 is 1.58 Å in ***R*-IM1**), which in turn is caused by the different positions of the fixed atoms.

We first investigated a path analogous to the RKCH mechanism for the *S* enantiomer. It starts with the transfer of H1 from O4 to C2 and our results showed that while moving H1 to C2, H2 moves concertedly to O6 and then to O2. However, this gives rise to the wrong enantiomer of the product. The energy barrier for this step (***R*-TS2**) is 12.0 kcal mol^{-1} and the product (**L-P**) is –6.7 kcal mol^{-1} below ***R*-R**. The overall barrier for this path is 19.1 kcal mol^{-1} (the energy profile is shown with blue in Figure 8). As for the first step, the overall energy of this path is close to the overall energy of RKCH path for the *S* substrate (19.1 vs. 21.5 kcal mol^{-1} for the *S* substrate). However, for the *R* substrate the second and the third steps take place concertedly.

We have also tested other possible paths starting from ***R*-IM1**. RK suggested that Glu-172 should abstract H2 from O1 and transfer it to C2 (Scheme 4). However, we could not find any stable structure for the proton transfer of H2 to Glu-172; instead, the structure returned to the starting point (***R*-IM1**) if the H2–O6 bond constraint is released. As for the *S* substrate, this is quite natural, because the substrate would then acquire a –2 charge. The structure with the H2–O6 bond constrained to 1.0 Å is shown in Figure 6 as ***R*-IM2-fixed**; it is 5.7 kcal mol^{-1} above ***R*-IM1** (see Figure 8).

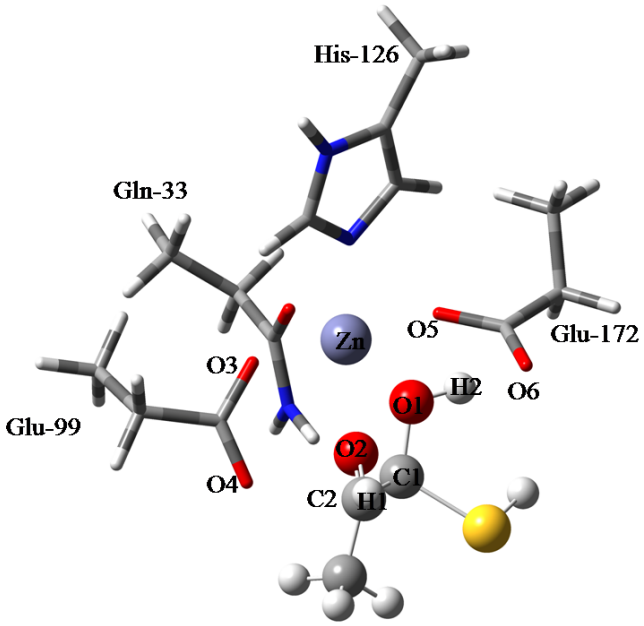

***R*-R**

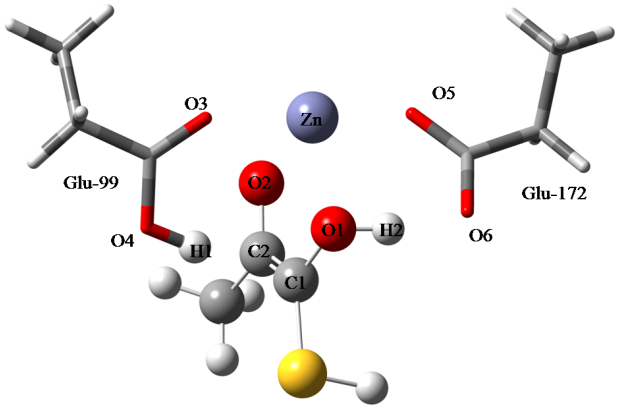

***R*-IM1**

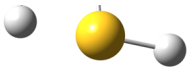

***R*-IM1**

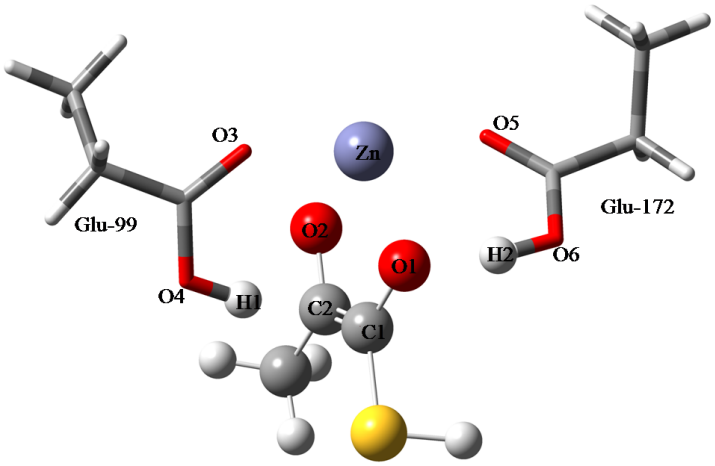

***R*-IM2-fixed**

Figure 6. Optimized structures of the first-order stationary points for the *R* substrate. All residues and atoms are shown for ***R*-R**, but for clarity only the Zn atom, the substrate and .the glutamate residues are shown for the other structures

HS proposed that after formation of ***R*-IM1**, H1 moves from Glu-99 to O2 (resulting in ***R*-IM2H**). Next, Glu-172 abstracts H2 from O1 (resulting ***R*-IM3H**) and transfers it to the *si* face of C2 to give **D-P** (cf. Scheme 5). We calculated an energy barrier for formation of ***R*-IM2H** from ***R*-IM1** (the TS is ***R*-TS2H**) of 1.0 kcal mol^{-1}. ***R*-IM2H** is 3.0 kcal mol^{-1} higher than ***R*-R**. The difference between ***R*-IM2H** and ***R*-IM3H** is in the movement of H2 within the hydrogen bond between O1 and O6 (see Figure 7 and Figure 8 for the structures and energies, respectively). ***R*-IM3H** is slightly higher in energy than ***R*-IM2H** (0.4 kcal mol^{-1}), but the transition state of this proton exchange (***R*-TS3H**) is 0.1 kcal mol^{-1} lower in energy than ***R*-IM3H**. The last step in the mechanism is movement of H2 from O6 to C2, resulting **D-P**. The energy barrier for the later step (the TS is ***R*-TS4H**) is relatively high (5.0 kcal mol^{-1}, but this is still below ***R*-TS1**) and **D-P** is –7.8 kcal mol^{-1} lower than ***R*-R**. Thus, this is a feasible reaction mechanism.

As for the *S* substrate, we also checked alternative paths in the HS mechanism for the *R* substrate (transferring H1 to Glu99 in ***R*-IM2H** and then to the *re* face of C2). The former step produces ***R*-IM3H-L** through ***R*-TS3H-L**. ***R*-IM3H-L** is slightly lower in energy than ***R*-IM2H** (0.2 kcal mol^{-1}). The transition state is 1.2 kcal mol^{-1} lower in energy than ***R*-IM3H-L**. When H1 moves to C2 in R-IM3H-L, H2 moves concertedly to Glu172 and then to O2,. This produces **L-P** trough ***R*-TS4H-L**. The energy barrier for the later step is 5.2 kcal mol^{-1}. Consequently, as can be seen in Figure 8, the overall energy barriers for production of the two enantiomers of the product are equal in this mechanism (10.5 kcal mol^{-1}, governed by ***R*-TS1**). However, the barrier for production of **L-P** from ***R*-IM2H** is slightly lower than the barrier of production of **D-P** product from ***R*-IM2H** (5.0 vs. 5.4 kcal mol^{-1}).

In conclusion, the HS mechanism for the *R* substrate seems reasonable. It does not contain any challenging steps (like the transformation of ***S*-IM2H** to ***S*-IM2H-ISO**) and both of the glutamates play a role in the mechanism. However, the two variants of the mechanism seem to lead to the production of the two enantiomers of the product with the same overall energy barriers, which is not in accordance with experimental data.

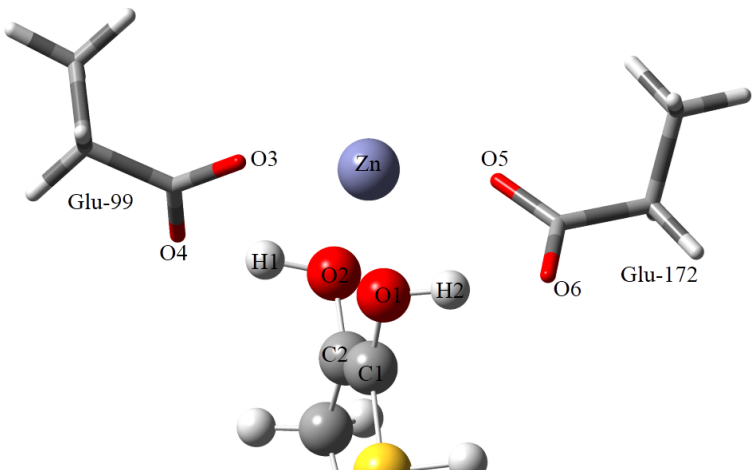

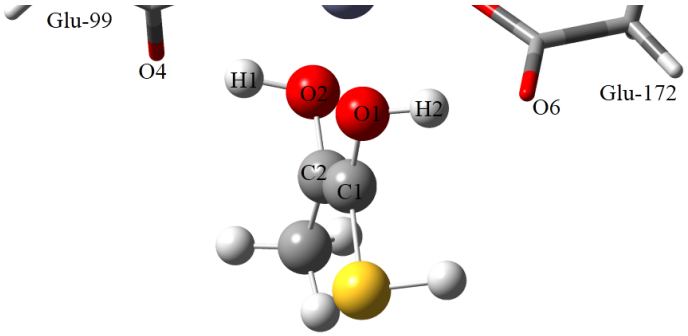

***R*-IM2H**

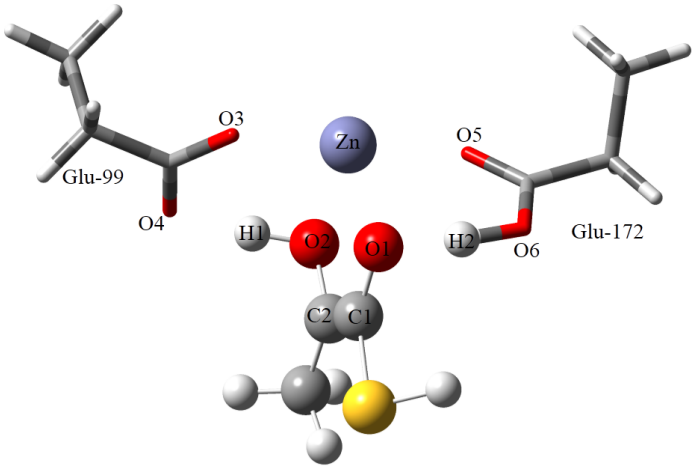

***R*-IM3H**

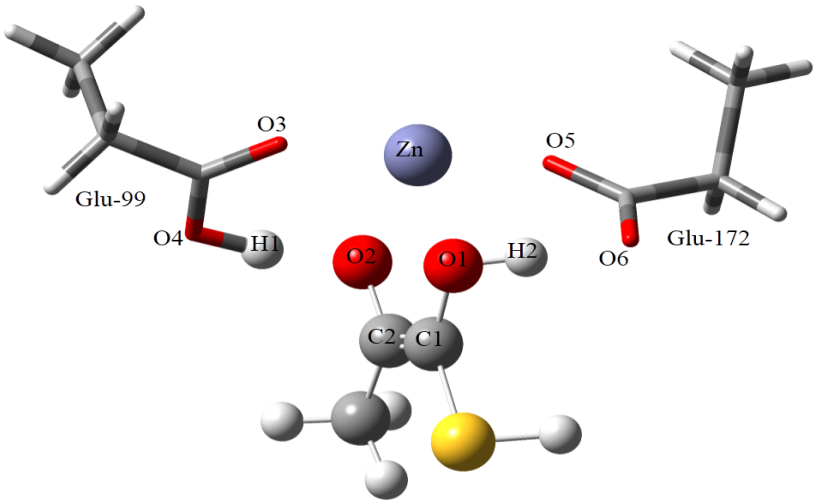

***R*-IM3H-L**

Figure 7. Optimized structures of the first order stationary points along the reaction pathway for the *R* substrate in the HS mechanism. For clarity, only the Zn atom, the substrate and the glutamate residues are shown.

Figure 8. Energy profile of the different paths for the *R* substrate reaction.

Finally, CH have suggested a dissociative mechanism in which the enzyme catalyzes the interconversion of the enantiomers prior to converting the *S* substrate to the product. However, this mechanism seems unlikely. A high-field ^{1}HNMR analysis revealed that the *R* and *S* enantiomers are both converted to glutathiohydroxyacetone (HOC-SG) at rates of 0.8 and 0.4 s^{-1}, respectively [41]. In other words, the *R* enantiomer reacts faster than the *S* enantiomer. However, the conversion of the *R* substrate prior the reaction will make the reaction of the *R* substrate slower than that of the *S* substrate.

Finally, CH have suggested a dissociative mechanism in which the enzyme catalyzes the interconversion of the enantiomers prior to converting the *S* substrate to the product. However, this mechanism seems unlikely. A high-field ^{1}HNMR analysis revealed that the *R* and *S* enantiomers are both converted to glutathiohydroxyacetone (HOC-SG) at rates of 0.8 and 0.4 s^{-1}, respectively [41]. In other words, the *R* enantiomer reacts faster than the *S* enantiomer. However, the conversion of the *R* substrate prior the reaction will make the reaction of the *R* substrate slower than that of the *S* substrate.

The overall energy barriers of the various paths calculated for the QM-cluster model in this study are summarized in Table 2 (compiled from the data in Figure 3 and Figure 8). It can be seen that our results indicate that the RKCH mechanism and its symmetric *R* variant are unfavorable for both the *S* and *R* substrates with activation barriers of 21.5 and 19.1 kcal mol^{-1}, respectively. On the other hand, the HS mechanisms give lower and more reasonable barriers for both substrates, 14.3, and 10.5 kcal mol^{-1}, respectively. However, alternative pathways leading to the incorrect isomer of the product, **L-P** (via **IM3H-L**), are competitive for both substrates. For the *R* substrate, this pathway has the same overall barrier as the HS mechanism, whereas for the *S* substrate, the barrier is 1.6 kcal mol^{-1} lower than for the HS mechanism. Thus, our calculations do not reflect the experimentally observed stereospecificity of the enzyme. The reason for this is most likely that our QM-cluster model is too symmetric, i.e. that the two glutamate models are too similar.

On the other hand, our calculations show some asymmetry: There are significant differences in the calculated barriers of the symmetry-related paths in Table 2, i.e. paths 1 and 4 or paths 3 and 5. Moreover, the HS mechanism for the *S* substrate is more complicated than path 6 (we have tried to find the symmetry-equivalent variant of path 6 also for the *S* substrate, i.e. transferring H1 from O2 to Glu172 in S-IM2H, but after releasing any bond constraints the structure returns to the starting point). As discussed previously, these differences are caused by the positions of the fixed atoms, which are influenced by the different coordination states of the glutamate residues in the starting crystal structure.

Table 2. Overall energy barriers of different paths for the model of this work in kcal mol^{-1}.

Path number	Path	Reactant enantiomer	Product enantiomer	Overall barrier
1	RKCH mechanism	*S*	D	21.5
2	HS mechanism	*S*	D	14.3
3	***S*-IM2H** to **L-P**	*S*	L	12.7
4	*R* variant of the RKCH mechanism	*R*	L	19.1
5	HS mechanism for *R* substrate	*R*	D	10.5
6	***R*-IM2H** to **L-P**	*R*	L	10.5

Apparently, these differences are not enough to introduce the observed stereospecificity of GlxI in the calculations, neither in this work nor in the previous studies [5,6]. Instead, the glutamates bind symmetrically to the metal center but their electronic effects and flexibility seem to be different. These differences could be related to the different surroundings of the glutamates. Interestingly, there is a flexible loop, including residues 152–159, over the active site in the crystal structure of GlxI, which is closer to Glu-172 than to Glu-99 [4]. This may give more freedom to Glu-172 to do the proton transfers. A witness of the different actions of the glutamate residues is the suggested protonation of Glu-172 in the HIC-SG complex, which also positioned this group further away from the Zn center. This indicates that Glu-172 can easily dissociate from Zn in the crystal structure by abstraction of a proton, whereas Glu-99 cannot.

In this context, it is notable that the enzyme also catalyzes the stereospecific exchange of the H_s proton of HOC-SG with solvent D_2O [42] (see Scheme 7). GlxI can pick up H_s but not H_r, although the protons seem to have the same chemical environment. If the glutamate residues of the active site are involved in this reaction, they must have different action in the active site.

To investigate the stereospecificity of GlxI, a very big QM cluster model is necessary, including all neighboring residues of the glutamates, which would be computationally very

In this context, it is notable that the enzyme also catalyzes the stereospecific exchange of the H_s proton of HOC-SG with solvent D_2O [42] (see Scheme 7). GlxI can pick up H_s but not H_r, although the protons seem to have the same chemical environment. If the glutamate residues of the active site are involved in this reaction, they must have different action in the active site.

To investigate the stereospecificity of GlxI, a very big QM cluster model is necessary, including all neighboring residues of the glutamates, which would be computationally very expensive. Alternatively, combined QM and molecular mechanics (QM/MM) calculations may be employed. Such a study is currently undertaken in our groups.

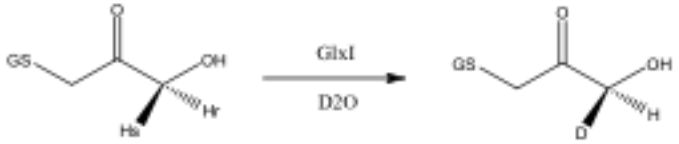

Scheme 7. Stereospecific exchange of the H_s proton of HOC-SG with solvent D_2O by GlxI

Conclusion

We have in this study performed DFT calculations on a model of the active site of GlxI, modeling the reactions for both the *S* and *R* forms of the substrate. Following the QM-cluster approach [28,32-34](27,31-33), we fixed four atoms in the model to their crystallographic positions (Figure 1). The results show that the coordination shell of the Zn ion in the optimized geometries is more symmetric than the HIC-SG crystal structure, with Glu-172 coordinating to the Zn ion in the optimized structure, but not in the crystal structure, probably owing to differences in the protonation states and the electronic structure of the HIC-SG inhibitor, compared to the substrate. We concluded that Glu-172 is protonated in the HIC-SG crystal structure.

We have compared on an equal footing two suggested mechanisms for the reaction of the *S* substrate, as well as several additional mechanisms. We show that the HS mechanism gives a lower barrier than the RKCH mechanism, although it is more complicated. However, the results also show that an alternative route, giving rise to the other stereoisomer of the product, has a slightly lower barrier than the HS mechanism. In all mechanisms, the two active site glutamate residues (Glu99 and Glu172) play significant roles, transferring the protons between the substrate carbon and oxygen atoms. This is in agreement with mutation studies, showing that the Glu172Gln and Glu99Gln mutants have activities that are $>10^5$ and $>10^4$ smaller than that of the wild-type enzyme, respectively [40]. The active-site Zn ion is also important for the mechanism by stabilizing the enediolate intermediate and the corresponding transition state.
The calculations for the *R* substrate showed that, like the *S* substrate, the coordination shell of the Zn ion is more symmetric than in the HIC-SG crystal structure. This symmetry indicates that the enzyme could use the same reaction mechanisms as for the *S* substrate, but with exchanged roles of Glu-99 and Glu-172. Consequently, our results show that the *R* variant of the RKCH mechanism gives a higher barrier than the HS mechanism and that an alternative mechanism leading to the **L-P** product gives the same overall barrier as the HS mechanism. Thus, our calculations do not reflect the experimentally observed stereospecificity of the enzyme, owing to the too symmetric model QM-cluster model used in this study. On the other hand, our calculations show some asymmetry, caused by the positions of the fixed atoms, which are influenced by the different coordination states of the glutamate residues in the starting crystal structure.

We propose that the stereospecificity of GlxI is caused by different environments of the glutamate residues in the active site, giving them different electronic effects and different flexibility owing to the neighboring residues. Our calculations also emphasize the importance of studying all steps in a suggested reaction mechanism (to see that it is really feasible) and also all possible side reactions (and not only the desired reaction mechanism), which can give rise to alternative reaction paths with lower barriers.

Acknowledgements
This investigation has been supported by grants from the Swedish research council (project 2014-5540). The computations were performed on computer resources provided by the Swedish National Infrastructure for Computing (SNIC) at Lunarc at Lund University.

which can give rise to alternative reaction paths with lower barriers.

Acknowledgements
This investigation has been supported by grants from the Swedish research council (project 2014-5540). The computations were performed on computer resources provided by the Swedish National Infrastructure for Computing (SNIC) at Lunarc at Lund University.

References

1. Frykman, H.; Öhrner, N.; Norin, T.; Hult, K. Tetrahedron Letters 1993, 34(8), 1367-1370.
2. Ayoub, F. M.; Allen, R. E.; Thornalley, P. J. Leukemia Research 1993, 17(5), 397-401.
3. Cameron, A. D.; Olin, B.; Ridderström, M.; Mannervik, B.; Jones, T. A. The EMBO Journal 1997, 16(12), 3386-3395.
4. Cameron, A. D.; Ridderström, M.; Olin, B.; Kavarana, M. J.; Creighton, D. J.; Mannervik, B. Biochemistry 1999, 38(41), 13480-13490.
5. Richter, U.; Krauss, M. Journal of the American Chemical Society 2001, 123(29), 6973-6982.
6. Himo, F.; Siegbahn, P. E. M. Journal of the American Chemical Society 2001, 123(42), 10280-10289.
7. Creighton, D. J.; Hamilton, D. S. Archives of Biochemistry and Biophysics 2001, 387(1), 1-10.
8. Day, P. N.; Jensen, J. H.; Gordon, M. S.; Webb, S. P.; Stevens, W. J.; Krauss, M.; Garmer, D.; Basch, H.; Cohen, D. The Journal of Chemical Physics 1996, 105(5), 1968-1986.
9. Worthington, S. E.; Krauss, M. Computers & Chemistry 2000, 24(3–4), 275-285.
10. Feierberg, I.; Cameron, A. D.; Åqvist, J. FEBS letters 1999, 453(1–2), 90-94.
11. Chen, S.-L.; Li, Z.-S.; Fang, W.-H. Journal of inorganic biochemistry 2012, 111(0), 70-79.
12. Liao, R.-Z.; Himo, F.; Yu, J.-G.; Liu, R.-Z. Journal of inorganic biochemistry 2010, 104(1), 37-46.
13. Manta, B.; Raushel, F. M.; Himo, F. The Journal of Physical Chemistry B 2014, 118(21), 5644-5652.
14. Himo, F.; Guo, J.-D.; Rinaldo-Matthis, A.; Nordlund, P. The Journal of Physical Chemistry B 2005, 109(42), 20004-20008.
15. Velichkova, P.; Himo, F. The Journal of Physical Chemistry B 2005, 109(16), 8216-8219.
16. Sevastik, R.; Himo, F. Bioorganic chemistry 2007, 35(6), 444-457.
17. Chen, S.-L.; Fang, W.-H.; Himo, F. The Journal of Physical Chemistry B 2007, 111(6), 1253-1255.
18. Chen, S.-L.; Fang, W.-H.; Himo, F. Theoretical Chemistry Accounts 2008, 120(4-6), 515-522.
19. Liao, R.-Z.; Yu, J.-G.; Raushel, F. M.; Himo, F. Chemistry – A European Journal 2008, 14(14), 4287-4292.
20. Liao, R.-Z.; Yu, J.-G.; Himo, F. Proceedings of the National Academy of Sciences 2010, 107(52), 22523-22527.
21. Liao, R.-Z.; Yu, J.-G.; Himo, F. Journal of inorganic biochemistry 2011, 105(7), 927-936.
22. Lind, M. E. S.; Himo, F. Angewandte Chemie 2013, 52(17), 4563-4567.
23. Georgieva, P.; Himo, F. Journal of Computational Chemistry 2010, 31(8), 1707-1714.
24. Bunrit, A.; Dahlstrand, C.; Olsson, S. K.; Srifa, P.; Huang, G.; Orthaber, A.; Sjöberg, P. J. R.; Biswas, S.; Himo, F.; Samec, J. S. M. Journal of the American Chemical Society 2015, 137(14), 4646-4649.
25. Huang, G.; Kalek, M.; Liao, R.-Z.; Himo, F. Chemical Science 2015, 6(3), 1735-1746.
26. Santoro, S.; Liao, R.-Z.; Marcelli, T.; Hammar, P.; Himo, F. The Journal of Organic Chemistry 2015, 80(5), 2649-2660.
27. Himo, F.; Siegbahn, P. E. Chemical Reviews 2003, 103(6), 2421-2456.
28. Noodleman, L.; Lovell, T.; Han, W.-G.; Li, J.; Himo, F. Chemical Reviews 2004, 104(2), 459-508.
29. Himo, F. Biochimica et Biophysica Acta (BBA)-Bioenergetics 2005, 1707(1), 24-33.
30. Himo, F. Theor Chem Account 2006, 116(1-3), 232-240.
31. Siegbahn, P. E.; Borowski, T. Accounts of chemical research 2006, 39(10), 729-738.
32. Ramos, M. J.; Fernandes, P. A. Accounts of Chemical Research 2008, 41(6), 689-698.
33. Siegbahn, P. M.; Himo, F. J Biol Inorg Chem 2009, 14(5), 643-651.
34. Lee, C.; Yang, W.; Parr, R. G. Physical Review B 1988, 37(2), 785-789.

28. Noodleman, L.; Lovell, T.; Han, W.-G.; Li, J.; Himo, F. Chemical Reviews 2004, 104(2), 459-508.
29. Himo, F. Biochimica et Biophysica Acta (BBA)-Bioenergetics 2005, 1707(1), 24-33.
30. Himo, F. Theor Chem Account 2006, 116(1-3), 232-240.
31. Siegbahn, P. E.; Borowski, T. Accounts of chemical research 2006, 39(10), 729-738.
32. Ramos, M. J.; Fernandes, P. A. Accounts of Chemical Research 2008, 41(6), 689-698.
33. Siegbahn, P. M.; Himo, F. J Biol Inorg Chem 2009, 14(5), 643-651.
34. Lee, C.; Yang, W.; Parr, R. G. Physical Review B 1988, 37(2), 785-789.
35. Frisch, M. J.; Trucks, G. W.; Schlegel, H. B.; Scuseria, G. E.; Robb, M. A.; Cheeseman, J. R.; Montgomery, J. A.; Vreven, T.; Kudin, K. N.; Burant, J. C.; Millam, J. M.; Iyengar, S. S.; Tomasi, J.; Barone, V.; Mennucci, B.; Cossi, M.; Scalmani, G.; Rega, N.; Petersson, G. A.; Nakatsuji, H.; Hada, M.; Ehara, M.; Toyota, K.; Fukuda, R.; Hasegawa, J.; Ishida, M.; Nakajima, T.; Honda, Y.; Kitao, O.; Nakai, H.; Klene, M.; Li, X.; Knox, J. E.; Hratchian, H. P.; Cross, J. B.; Bakken, V.; Adamo, C.; Jaramillo, J.; Gomperts, R.; Stratmann, R. E.; Yazyev, O.; Austin, A. J.; Cammi, R.; Pomelli, C.; Ochterski, J. W.; Ayala, P. Y.; Morokuma, K.; Voth, G. A.; Salvador, P.; Dannenberg, J. J.; Zakrzewski, V. G.; Dapprich, S.; Daniels, A. D.; Strain, M. C.; Farkas, O.; Malick, D. K.; Rabuck, A. D.; Raghavachari, K.; Foresman, J. B.; Ortiz, J. V.; Cui, Q.; Baboul, A. G.; Clifford, S.; Cioslowski, J.; Stefanov, B. B.; Liu, G.; Liashenko, A.; Piskorz, P.; Komaromi, I.; Martin, R. L.; Fox, D. J.; Keith, T.; Laham, A.; Peng, C. Y.; Nanayakkara, A.; Challacombe, M.; Gill, P. M. W.; Johnson, B.; Chen, W.; Wong, M. W.; Gonzalez, C.; Pople, J. A., 2003.
36. Hay, P. J.; Wadt, W. R. The Journal of Chemical Physics 1985, 82(1), 270-283.
37. Barone, V.; Cossi, M. The Journal of Physical Chemistry A 1998, 102(11), 1995-2001.
38. Reed, A. E.; Weinhold, F. The Journal of Chemical Physics 1983, 78(6), 4066-4073.
39. Reed, A. E.; Curtiss, L. A.; Weinhold, F. Chemical Reviews 1988, 88(6), 899-926.
40. Ridderström, M.; Cameron, A. D.; Jones, T. A.; Mannervik, B. Journal of Biological Chemistry 1998, 273(34), 21623-21628.
41. Landro, J. A.; Brush, E. J.; Kozarich, J. W. Biochemistry 1992, 31(26), 6069-6077.
42. Chari, R. V. J.; Kozarich, J. W. Journal of the American Chemical Society 1983, 105(24), 7169-7171.